Available online at www.sciencedirect.com
ScienceDirect
Journal of Computational Physics 218 (2006) 228–245
JOURNAL OF COMPUTATIONAL PHYSICS
www.elsevier.com/locate/jcp

Fourth-order balanced source term treatment in central WENO schemes for shallow water equations

V. Caleffi *, A. Valiani, A. Bernini

Università degli Studi di Ferrara, Dipartimento di Ingegneria, Via G. Saragat, 1, 44100 Ferrara, Italy

Received 22 March 2005; received in revised form 1 February 2006; accepted 4 February 2006
Available online 20 March 2006

Abstract

The aim of this work is to develop a well-balanced central weighted essentially non-oscillatory (CWENO) method, fourth-order accurate in space and time, for shallow water system of balance laws with bed slope source term. Time accuracy is obtained applying a Runge–Kutta scheme (RK), coupled with the natural continuous extension (NCE) approach. Space accuracy is obtained using WENO reconstructions of the conservative variables and of the water-surface elevation. Extension of the applicability of the standard CWENO scheme to very irregular bottoms, preserving high-order accuracy, is obtained introducing two original procedures. The former involves the evaluation of the point-values of the flux derivative, coupled with the bed slope source term. The latter involves the spatial integration of the source term, analytically manipulated to take advantage from the regularity of the free-surface elevation, usually smoother than the bottom elevation. Both these procedures satisfy the C-property, the property of exactly preserving the quiescent flow. Several standard one-dimensional test cases are used to verify high-order accuracy, exact C-property, and good resolution properties for smooth and discontinuous solutions.

MSC: 35L65; 65D05; 76M20

Keywords: High-order methods; CWENO schemes; Shallow water equations; Source terms; C-property

1. Introduction

In recent years, high resolution methods for hyperbolic systems of conservation laws have been extensively applied to shallow water equations to solve problems in fluid mechanics and hydraulic engineering [32,1,24]. In particular, finite volume methods of the Godunov class have reached a quite mature stage and therefore it is possible to use them in different practical engineering applications [31,36,5]. In most part of such applications,

* Corresponding author. Fax: +39 0532 974870.
E-mail addresses: valerio.caleffi@unife.it, vcaleffi@ing.unife.it (V. Caleffi), alessandro.valiani@unife.it (A. Valiani), anna.bernini@unife.it (A. Bernini).

0021-9991/$ - see front matter
doi:10.1016/j.jcp.2006.02.001

second-order accuracy in time and space is used, as the optimal compromise between a reasonable grid refinement and an acceptable complexity of numerical schemes.

From the point of view of basic research, hyperbolic systems of conservation laws are recently faced with the specific purpose of using coarse grids for numerical integration, so that an increasing order of accuracy is used. A very important class of high accuracy numerical methods, starting from the pioneering work of Harten et al. [9], is ENO (essentially non-oscillatory) methods, which have rapidly grown toward WENO (weighted essentially non-oscillatory) methods: the works of Liu et al. [23] and Jiang and Shu [13] are the cornerstones in this field. A complete description of WENO schemes is included in the review by Shu [30].

Inside ENO and WENO classes of methods, two principal approaches can be distinguished. The classical one is the upwind approach, again due to Godunov [8], in which the eigensystem is extensively used. The main advantage of this method is its strong physical basis, which allows to obtain a very good resolution and the maximum reduction of unphysical oscillations near the shocks. The alternative approach is the centered scheme family, whose origins are the first-order Lax–Friedrichs [18] staggered method and the second-order Nessyahu–Tadmor [25] staggered method. The eigensystem is ignored by these methods. Qiu and Shu [28] perform a comparison between central staggered and upwind non-staggered WENO high-order methods, which use or do not use the local characteristic decomposition. In this analysis, such a decomposition is shown to improve results when the structure of the shocks is more complex and the order of accuracy of the method is very high. On the other hand, the need to know the eigensystem represents a strong limit to upwind schemes versatility. In fact, central WENO schemes (CWENO) [30,12,20,27] are particularly useful when standard form of equations is abandoned for a more complex structure of equations. In this case, the eigensystem may be very complex or even unknown. For example, this may be the case in fluvial hydraulics, when the purpose is the hydrodynamical and morphological modelling of flow in meandering rivers and secondary flows cannot be neglected [29,15,11]. Other cases in which the eigensystem may be very complex are when a flow with intense sediment transport, mud flow or debris flow, occur and the propagation celerity of the bulk flow is affected by the solid concentration [6].

Two important contributions on CWENO approach are due to Levy et al. [20,21], which present a new family of schemes for approximating solutions of hyperbolic systems of conservation laws, for one-dimensional and two-dimensional problems. The fundamental keys of these methods are the reconstruction of the point-values of conservative variables, the reconstruction of the flux derivatives and the combination of the natural continuous extension (NCE, [41]) procedure with a Runge–Kutta solver in time. Such methods are the extension to third and fourth-order accuracy of the classical second-order Nessyahu–Tadmor [25] scheme and its multi-dimensional version [14]. The independence from the eigensystem of the scheme and the consequent component-wise structure are described as the main advantages of Levy et al. [20,21] methods.

Several works are recently devoted to the consistent numerical treatment of source term due to bed slope of shallow flow equations, to allow the application of WENO methods to engineering problems. Such a term may be a strong cause of instability, provided that bottom elevation is often irregular in real topography.

A recent work by Vuković and Sopta [38], which is specifically devoted to the numerical integration of the shallow water equations, applies, in a ENO–WENO context, the idea of balancing the momentum flux with the source term. Such a method has been introduced by Bermudez and Vázquez-Cendón [3] and then improved by Vázquez-Cendón [37]. On the same research line, the work by Garcia-Navarro and Vázquez-Cendón [7], which analyzes the source term due to cross section irregularities, and the work by Hubbard and Garcia-Navarro [10], which analyzes the effects of source terms in a flux difference splitting technique, can be mentioned. In Vuković and Sopta [38], the *C-property* [3,37] is exactly satisfied, but the complexity of the method is relevant. A different approach is adopted in the quasi-steady wave propagation method by LeVeque [19]. In this method, in order to obtain balancing, a Riemann problem in the center of each cell is introduced.

In the different context of finite difference WENO scheme, Xing and Shu [40] develop a treatment for bed slope source term which satisfies the C-property and, at the same time, maintains genuine high-order accuracy. Such a treatment can be applied to one- and two-dimensional problems. High accuracy and well-balancing are also obtained by Črnjarić-Žic et al. [33] using both finite volume WENO and central WENO schemes. In particular, Črnjarić-Žic et al. [33] apply their schemes not only to SWE but also to De Saint-Venant open-channel

flow equations where source terms depend on the channel geometry. In a finite volume context, their balancing technique involves the cell-integral of source term and depends on the selected approximate Riemann solver (Roe's Riemann solver). In the central schemes context, the balancing technique involves the evaluation both of the source term point-values and the source term cell-averages.

Good results are also obtained adopting the DFB method (divergence form for the bed slope source term, [34]). Such a method consists of writing the product of the flow depth times the bed slope as the divergence of a properly defined tensor, in which the static force due to the non-horizontality of the bed is taken into account. In one-dimensional computations, bed slope source term is written as the derivative of half the square of the flow depth, provided that the free-surface elevation inside each cell is a proper constant over the cell itself. In the original paper, Valiani and Begnudelli [34] have shown an enormous increasing in stability in several appropriate test cases, both in one and two dimensions.

Important contributions towards the proper simulation of real cases are given using unstructured grids, which are necessary to reproduce flows over computational domains characterized by complex boundaries. Kurganov and Petrova [17] have extended the semi-discrete central-upwind schemes [16], which are based on the use of local propagation celerities, to triangular grids in 2D problems. The use of the semi-discrete form allows to avoid grid staggering, introducing significant simplifications when multi-dimensional problems must be faced. In a more recent work, Bryson and Levy [4] extended the same scheme to allow its application to SWE with bed slope source term.

Multi-dimensional computations are performed using a Nessyahu–Tadmor [25] method modified by Arminjon and St-Cyr [2], which use a structured grid in two dimensions and an unstructured grid in three dimensions. Their central scheme avoid an intermediate predictor-step between time t^n and t^{n+1}, increasing the computational efficiency and preserving the resolution of shock and rarefaction waves typical of the original Nessyahu–Tadmor scheme. 3D cartesian, adaptive grids are discussed in Noelle et al. [26]. An adaptively refined primal grid coupled with a dual grid based on L^∞-Voronoi cells are used. The selected geometrical structure shows to save computational time. At the moment the scheme is first-order accurate but its general structure is conceived to be extended to the second order using a Nessyahu–Tadmor scheme.

The original contribution of the present work regards the proper numerical treatment of bed slope source term for high accuracy, well-balanced, central WENO methods. The novel approach is presented in the context defined in [20,21,12] and involves three different aspects of the scheme: the WENO reconstructions are reformulated according to the surface gradient method [42], i.e., the free-surface elevation is used instead of the flow depth; the numerical approximation of the point-values of flux derivative and of source term is defined to obtain the balancing between the flux gradient and the source term itself, preserving high accuracy; the cell-integral of source term is defined to obtain high accuracy and well-balancing. The designed scheme assures the fulfillment of the following conditions: the full achievement of fifth-order spatial accuracy; the full achievement of fourth-order time accuracy; the complete consistence with the CWENO philosophy; the satisfaction of the exact C-property; a sufficient robustness of the scheme, which limits the generation of spurious oscillations when complex and irregular bed configuration occurs. The last requirement is significant in order to obtain a versatile tool, whose performances are not problem dependent.

In this paper only one-dimensional flow is considered, in order to verify the introduced novelties over simple, well established test cases. However, the strength of the present method consists of a large applicability in a broad range of engineering problems. In particular, the method may be applied in civil engineering problems where simulations of river flows, debris flows, mud flows, real world dam break waves, flood waves, etc. (see [35,5,36] and the references therein) are currently performed using 1D and 2D numerical models based on SWE. For example, the case of fixed bed is analyzed, but it is simple to extend the present concepts to the movable bed case (see also Valiani et al. [35], for preliminary examples). The new ideas presented in this work can be also extended to 2D problems because the structure of the 2D SWE and the corresponding source term are similar to the 1D version of the same equation.

Several standard one-dimensional test cases are used to verify high-order accuracy, the exact C-property, and the good resolution for smooth and discontinuous solutions. The method is proved to be the natural extension, for shallow water flows with arbitrary bed elevation, of Levy et al. [20] method.

2. Numerical model

The presented numerical model is developed starting from the explicit fourth-order central WENO scheme proposed by Levy et al. [20], which is suitable for the numerical integration of homogeneous systems of conservation laws. To avoid any ambiguity in the discrete description of bed profile in staggered schemes – due to the use of two different, coupled grids – the destaggering procedure presented in [12] is applied. In this work the scheme is extended in order to treat the one-dimensional SWE with only the geometrical source term. Friction slope source term is not treated in this work.

Assuming classical hypothesis [22], 1D shallow water equations may be written as:

$$u_t + f_x = s \quad \Longleftrightarrow \quad \frac{\partial}{\partial t}\begin{bmatrix} h \\ vh \end{bmatrix} + \frac{\partial}{\partial x}\begin{bmatrix} vh \\ gh^2/2 + v^2 h \end{bmatrix} = \begin{bmatrix} 0 \\ ghs_0 \end{bmatrix}, \tag{1}$$

where $u(x,t)$ is the vector of conservative variables; $f(u(x,t))$ is the flux vector; $s(x,u(x,t))$ is the source term relative to the bottom slope. t is the time, x is the space, $h(x,t)$ is the flow depth, $v(x,t)$ is the vertically averaged velocity, g is the gravity, $s_0 = -\mathrm{d}z/\mathrm{d}x$ is the bottom slope and $z(x)$ is the bottom elevation.

Here and in the following, each vector operation must be intended *component-wise*.

Spatial discretization of the computational domain is based on a spatial step Δx, an uniformly spaced grid defined by $x_j = j\Delta x$, and a staggered grid defined by $x_{j+1/2} = (j + 1/2)\Delta x$. Each computational step is characterized by a time interval Δt^n, which is selected in order to assure the stability of the numerical scheme (see Section 2.1). t^n is the time level of the known variables, while $t^{n+1} = t^n + \Delta t^n$ is the time level of the unknown variables. Denoting: $I_j = [x_{j-1/2}, x_{j+1/2}]$ the jth cell, centered around the grid point x_j; $\bar{u}_j^n$ the corresponding cell-averaged solution at time t^n; $\bar{s}_j$ the cell-averaged source term, the integration of Eq. (1) over $[x_j, x_{j+1}] \times [t^n, t^{n+1}]$ gives:

$$\bar{u}_{j+1/2}^{n+1} = \bar{u}_{j+1/2}^{n} - \frac{1}{\Delta x}\int_{t^n}^{t^{n+1}} \left[f(u(x_{j+1},t)) - f(u(x_j,t))\right] \mathrm{d}t + \int_{t^n}^{t^{n+1}} \bar{s}_{j+1/2}\, \mathrm{d}t. \tag{2}$$

Eq. (2) describes the advancing from the time level t^n to the time level t^{n+1} in staggered central WENO schemes. The known state of the system, given through the cell-averaged solution on the original grid, is updated on the shifted grid. In the non-staggered version of central WENO schemes [12] an additional step is added and the updated solution $\bar{u}_{j+1/2}^{n+1}$ is projected back on the original grid, obtaining $\bar{u}_j^{n+1}$.

In order to allow the effective discretization of Eq. (2), it is necessary to design [20,27,40]:

- a reconstruction of the variables to evaluate the cell-averaged values on the staggered grid, starting from cell-averaged values on the non-staggered grid and vice versa;
- a well-balanced spatial integration of source term;
- a reconstruction of the variables to determine the point-values in the cell-centers;
- a well-balanced reconstruction to evaluate the point-value flux derivatives coupled to the source term.

As explained in the following, the last two reconstructions are needed for the time integration.

2.1. Time integration

The staggering of the grid is particularly useful for the time integration of the balance laws. In fact, time integrals are evaluated in the cell-centers of the non-staggered grid, where the solution is smooth. Such a condition allows to adopt standard numerical techniques for the time integral approximation [30,12,20]. In order to achieve the fourth-order accuracy in time, a Simpson's quadrature rule is selected [20]. According to this assumption, time integrals of Eq. (2) become:

$$\bar{u}_{j+1/2}^{n+1} = \bar{u}_{j+1/2}^{n} - \frac{\Delta t^n}{\Delta x}\sum_{l=1}^{3} N_l \left[f(\hat{u}(x_{j+1}, t^n + \beta_l \Delta t^n)) - f(\hat{u}(x_j, t^n + \beta_l \Delta t^n)) - \Delta x \bar{s}_{j+1/2}^{n+\beta_l}\right] \tag{3}$$

with

$$\bar{s}_{j+1/2}^{n+\beta_l} = \frac{1}{\Delta x}\int_{x_j}^{x_{j+1}} s(x, t^n + \beta_l \Delta t^n)\,\mathrm{d}x. \tag{4}$$

$N = [1/6,2/3,1/6]^{\mathrm{T}}$ are the weights and $\beta = [0,1/2,1]^{\mathrm{T}}$ are the nodes of the quadrature; $\hat{u}$ is the estimated point-value solution, see [20].

The approximation of the point-value solution at time t^{n+1}, appearing in Eq. (3), is performed by a fourth-order Runge–Kutta scheme and it is expressed by:

$$\hat{u}^{n+1} = \hat{u}^n + \Delta t^n \sum_{i=1}^{4} b_i k^{(i)} \quad \text{and} \quad \hat{u}^{(i)} = \hat{u}^n + \Delta t^n \sum_{j=1}^{i} a_{ij} k^{(j)}, \tag{5}$$

where

$$b = \begin{bmatrix} 1/6 \\ 1/3 \\ 1/3 \\ 1/6 \end{bmatrix}; \quad a = \begin{bmatrix} 0 & 0 & 0 & 0 \\ 1/2 & 0 & 0 & 0 \\ 0 & 1/2 & 0 & 0 \\ 0 & 0 & 1 & 0 \end{bmatrix} \tag{6}$$

and $k^{(i)}$ are the Runge–Kutta fluxes. For the considered balance law (1), $k^{(i)}$ is a numerical evaluation of $(-f_x + s)$, computed starting from the point-values $\hat{u}^{(i)}$. The Runge–Kutta fluxes computation is performed using an original approach described in Section 2.2.2, which allows the satisfaction of C-property.

The evaluation of the point-value at time $t^{n+1/2}$, appearing in Eq. (3), is obtained using the natural continuous extension [41,20,27] inside RK method:

$$\hat{u}^{n+1/2} = \hat{u}^n + \Delta t^n \sum_{i=1}^{4} B_i k^{(i)} \tag{7}$$

with $B = [5/24,1/6,1/6,-1/24]^{\mathrm{T}}$.

In order to assure numerical stability, an adaptive time step, satisfying the CFL-like condition, is selected [20]:

$$\Delta t^n = C\frac{\Delta x}{\max_j\left(|\hat{v}_j^n| + \sqrt{g\hat{h}_j^n}\right)}. \tag{8}$$

where $\hat{h}_j^n$ and $\hat{v}_j^n$ are the reconstructed point-values of flow depth and flow velocity at time t^n (see Section 2.2.1). $C = 0.35$ is a constant. This is the only point of the scheme in which a *rough* estimate of the eigenvalues of the system is needed.

2.2. WENO reconstructions

The surface gradient method (SGM) of Zhou et al. [43] is used and consequently the free-surface level $\eta = h + z$ is chosen here as the basis for the WENO reconstruction. This choice provides accurate point-values of the conservative variables at cell-centers and the achievement of the well-balancing between flux gradient and bottom slope source term. The vector of reconstructed variables $\mu = [\eta,hv]^{\mathrm{T}}$ is introduced.

2.2.1. Reconstruction of staggered cell-averaged and of non-staggered point-value conservative variables

The computation of the RHS of Eq. (3) requires the evaluation of the staggered cell-averages, $\bar{u}_{j+1/2}^n$, starting from the non-staggered cell-averages $\bar{u}_j^n$. Similarly, the time integration procedure described in Section 2.1, Eq. (5), requires the evaluation of the point-values $\hat{u}_j^n$, starting from the cell-averaged values $\bar{u}_j^n$. This section concerns the reconstruction needed for both these purposes [20,28,30].

The time level specifications are omitted to simplify the notation.
The procedure can be summarized in the following three steps:

(1) The cell-averaged values $\bar{\mu}_j$ are computed adding to the first component of $\bar{u}_j$ the cell-averaged values of bottom elevation $\bar{z}_j$.
(2) $R_j(x)$, suitable polynomials of degree 2, are defined and the pursued reconstruction is a piecewise function over the mesh I_j:

$$T(x) = \sum_j R_j(x)\chi_j, \tag{9}$$

where χ_j is the characteristic function of the interval I_j. Once $T(x)$ is given, $\bar{\mu}_{j+1/2}$ is computed using:

$$\bar{\mu}_{j+1/2} = \int_{x_j}^{x_{j+1}} T(x)\,\mathrm{d}x = \int_{x_j}^{x_{j+1/2}} R_j(x)\,\mathrm{d}x + \int_{x_{j+1/2}}^{x_{j+1}} R_{j+1}(x)\,\mathrm{d}x \tag{10}$$

and $\hat{\mu}_j$ is computed using:

$$\hat{\mu}_j = T(x_j) = R_j(x_j). \tag{11}$$

(3) Cell-averaged values $\bar{u}^n_{j+1/2}$ are computed by subtracting to the first component of $\bar{\mu}^n_{j+1/2}$ the cell-averaged values of bottom elevation $\bar{z}_{j+1/2}$. Point-values of $\hat{u}^n_j$ are computed by subtracting to the first component of $\hat{\mu}^n_j$ the point-values of bottom elevation z_j.

The reconstruction $T(x)$ must satisfy *conservation*, *accuracy* and *non-oscillation* requirements.

Conservation requirement: The following relation must hold:

$$\frac{1}{\Delta x}\int_{x_{j-1/2}}^{x_{j+1/2}} T(x)\,\mathrm{d}x = \frac{1}{\Delta x}\int_{x_{j-1/2}}^{x_{j+1/2}} R_j(x)\,\mathrm{d}x = \bar{\mu}_j. \tag{12}$$

Accuracy requirement: The following relations must hold:

$$\frac{1}{\Delta x}\int_{x_j}^{x_{j+1}} T(x)\,\mathrm{d}x = \frac{1}{\Delta x}\int_{x_j}^{x_{j+1}} \mu(x,t)\,\mathrm{d}x + \mathrm{O}(\Delta x^5) \tag{13}$$

and

$$T(x_j) = R_j(x_j) = \mu(x_j,t) + \mathrm{O}(\Delta x^5). \tag{14}$$

Non-oscillation requirement: The reconstruction must be essentially non-oscillatory [9,23,30], i.e., the magnitude of the oscillations near the discontinuities (*Gibbs phenomena*), is required to decay as $\mathrm{O}(\Delta x^k)$, where k is the selected order of accuracy of the scheme (in this work $k = 5$).

In order to fulfill these requirements, the following steps may be performed [20,28,27].
Three sets of three cells (*stencils*) $\mathscr{P}_{j+k} = \cup_{l=-1}^{l=+1} I_{j+k+l}$, with $k = -1, 0, 1$, are selected. The cell I_j belongs to each of them. Three polynomials of degree 2, $P_{j+k}(x)$, with $k = -1, 0, 1$, are introduced. Each polynomial is associated with a corresponding stencil $\mathscr{P}_{j+k}$. The cell-average of $P_{j+k}(x)$ in each cell of the stencil $\mathscr{P}_{j+k}$ is equal to the cell-average of the conservative variables, i.e.,

$$\frac{1}{\Delta x}\int_{I_{j+k-i}} P_{j+k}(x)\,\mathrm{d}x = \bar{\mu}_{j+k-i}, \qquad k = -1,0,1, \quad i = -1,0,1. \tag{15}$$

The coefficients of each polynomial $P_{j+k}(x)$ are uniquely determined by Eq. (15).
To satisfy the non-oscillatory requirement, the polynomial $R_j(x)$ is written as a convex combination of the three polynomials $P_{j+k}(x)$, using suitable variable *weights*, w^k_j $(k = -1, 0, 1)$. Such weights are functions of the solution regularity on each stencil $\mathscr{P}_{j+k}$:

$$R_j(x) = \sum_{k=-1}^{1} w^k_j P_{j+k}(x). \tag{16}$$

To compute w_j^k, the *linear weights* C_k and the *index of smoothness* function IS_j^k are introduced [28]. The linear weights are chosen such that the reconstruction satisfies the accuracy requirement, where the solution is smooth (see Table 1), while the index of smoothness function allows the optimal weighting of polynomials $P_{j+k}(x)$ in Eq. (16), where the solution is discontinuous.

Several expressions can be used to quantify the index of smoothness inside the stencil [23,13]. In this work the L^2-norm of the polynomial derivatives, $P_{j+k}^{(l)}(x)$ on the cell I_j, is selected, as suggested in [13]:

$$\mathrm{IS}_j^k = \sum_{l=1}^{2} \int_{I_j} \Delta x^{2l-1} \left(P_{j+k}^{(l)}\right)^2 \mathrm{d}x. \tag{17}$$

Finally, the indices of smoothness are used inside the final expressions for the weights:

$$\alpha_j^k = \frac{C_k}{\left(\epsilon + \mathrm{IS}_j^k\right)^p} \quad \text{and} \quad w_j^k = \frac{\alpha_j^k}{\sum_{l=-1}^{l=1} \alpha_j^l}, \tag{18}$$

where ϵ and p are empirically selected constants. The dimensional nature of ϵ and p parameters implies that *universal* values of these quantities *do not* exist, and problem-dependent values must be chosen. A detailed analysis has shown that this choice must be oriented to minimize numerical diffusion due to the staggering.

2.2.2. Reconstruction of Runge–Kutta fluxes

The evaluation of Runge–Kutta fluxes, necessary in Eq. (5), is performed by an original approach obtained modifying the reconstruction of flux derivative point-values introduced in classical CWENO schemes [20]. This approach, inspired also by the work of Črnjarić-Žic et al. [33], allows the C-property achievement.

The key element is the introduction of a proper cell function $K_j(x,u(x,t))$ defined by:

$$K_j(x,u(x,t)) = -\begin{bmatrix} (vh) - (vh)_j \\ (v^2h + 1/2g(\eta - z)^2) - (v^2h + 1/2g(\eta - z)^2)_j \end{bmatrix} + \begin{bmatrix} 0 \\ 1/2g((\eta_j - z)^2 - (\eta_j - z_j)^2) \end{bmatrix}. \tag{19}$$

Such a function $K_j(x,u(x,t))$ is conceived because it satisfies the following two analytical relations:

$$\left.\frac{\partial K_j}{\partial x}\right|_{x=x_j} = k_j = (-f_x + s)_j \tag{20}$$

and, for quiescent flow (i.e., $vh = 0$ and $\eta = \text{constant}$):

$$K_j(x) = 0 \quad \forall x. \tag{21}$$

Naming $T(x)$ the reconstruction of K_j, defined by an equation formally identical to (9), the Runge–Kutta fluxes on the grid x_j should be approximated by $T'(x_j)$ (i.e., $k_j \approx T'(x_j)$). This is a direct consequence of relation (20). The fulfillment of (21) assures the well-balancing between the flux gradient and the source term, as explained in Section 2.4.2.

The polynomials $R_j(x)$ are defined imposing *accuracy* and *non-oscillation* requirements (see Section 2.2.1). Here the accuracy condition (similarly to Eqs. (13) and (14)) is given by:

$$T'(x_j) = R_j'(x_j) = k_j + \mathrm{O}(\Delta x^4). \tag{22}$$

It is important to note that in classical CWENO schemes [13,28] the fourth-order accuracy in the evaluation of flux derivatives is sufficient to obtain the fifth-order spatial accuracy of the whole schemes. Similarly,

Table 1
Linear weights

	C_{-1}	C_0	C_{+1}
Cell-averaged and point value variables (see Section 2.2.1)	3/16	5/8	3/16
RK fluxes and free-surface derivatives (see Sections 2.2.2 and 2.3.1)	1/6	2/3	1/6
Cell-averaged ξ values (see Section 2.3.2)		1/2	1/2

fourth-order accuracy in the evaluation Runge–Kutta fluxes is sufficient for an overall fifth-order spatial accuracy of the presented method.

Let us consider three polynomials $P_{j+k}(x)$ of degree 2, related to the stencils $\mathscr{P}_{j+k}$. Their coefficients are univocally determined by imposing the passage of $P_{j+k}(x)$ through the three point-values of K_j, computed on the cell-centers of the respective stencils:

$$P_{j+k}(x_{j+k+l}) = K_j(x_{j+k+l}, \hat{u}^{(i)}_{j+k+l}), \qquad k = -1, 0, 1, \quad l = -1, 0, 1. \tag{23}$$

The polynomial $R_j(x)$ is written as a linear convex combination of the three polynomials $P_{j+k}(x)$, using suitable weights, w_j^k (see Eq. (16)). Such weights are computed using Eq. (18), with a specific set of linear weights (see Table 1). The computation of the linear weights is performed following the approach adopted in classical CWENO scheme for the computation of flux derivatives, see, for example [20,28,27]. The related IS_j^k are computed using Eq. (17), in which $P_{j+k}(x)$ are obtained starting from the point-values of the function K_j. This procedure leads to a fourth-order reconstruction of the Runge–Kutta fluxes.

2.3. Source term spatial integration

The novel technique for the numerical integration in space of the source term, appearing in Eq. (4), is described in this section. This integration must be performed at time t^n, $t^{n+1/2}$ and t^{n+1}. The principal aims of the new procedure are the achievement of high-order accuracy and the well-balancing.

The first step consists of the analytical manipulation of the second component of bed slope source term integration:

$$\bar{s}^{[2]}_{j+1/2}\Delta x = -\int_{x_j}^{x_{j+1}} gh\frac{\mathrm{d}z}{\mathrm{d}x}\,\mathrm{d}x, \tag{24}$$

using the relation $h = \eta - z$ and a simple integration by parts:

$$\begin{aligned}\bar{s}^{[2]}_{j+1/2}\Delta x &= -\int_{x_j}^{x_{j+1}} gh\frac{\mathrm{d}z}{\mathrm{d}x}\,\mathrm{d}x = -\int_{x_j}^{x_{j+1}} g(\eta - z)\frac{\mathrm{d}z}{\mathrm{d}x}\,\mathrm{d}x \\ &= \frac{1}{2}g\left[z_{j+1}^2 - z_j^2\right] - g\left[\eta_{j+1}z_{j+1} - \eta_j z_j\right] + \int_{x_j}^{x_{j+1}} gz\frac{\mathrm{d}\eta}{\mathrm{d}x}\,\mathrm{d}x\end{aligned} \tag{25}$$

and introducing $\xi(x) = gz\,\mathrm{d}\eta/\mathrm{d}x$:

$$\bar{s}^{[2]}_{j+1/2}\Delta x = \frac{1}{2}g\left[z_{j+1}^2 - z_j^2\right] - g\left[\eta_{j+1}z_{j+1} - \eta_j z_j\right] + \int_{x_j}^{x_{j+1}} \xi(x)\,\mathrm{d}x. \tag{26}$$

Eqs. (24) and (26) are analytically equivalent but, from the numerical point of view, they are different. In the former case the integration involves the bed spatial derivatives, while in the latter case the integration involves the free-surface spatial derivatives. In the case of irregular bottom, the latter formulation is preferable because the spatial derivative of free-surface elevation is more regular than the spatial derivative of the bed elevation, even if the solution is discontinuous. Finally, the overall error introduced in the numerical computation is smaller. In the case of regular bottom the two approaches are similar and, again, the formulation of Eq. (26) can be used. In this work the integration of source term is performed starting from Eq. (26).

At time t^n, $t^{n+1/2}$ and t^{n+1}, the discretization of the first two terms of the RHS of Eq. (26) does not present difficulties because they can be exactly computed from the point-values z_j and $\hat{\eta}_j$; only the last term requires an ad hoc numerical treatment. This integration is performed in three steps: the point-value derivatives $\hat{\eta}'_j$ are reconstructed starting from the point-values of $\hat{\eta}_j$; the point values of $\hat{\xi}_j = (gz\,\mathrm{d}\eta/\mathrm{d}x)_j$ is evaluated on this basis; the integral is computed using an original WENO reconstruction. All the steps fulfill the WENO requirements, as explained in the following sections.

2.3.1. Reconstruction of the point-values of the derivatives of free-surface elevation

At each time, t^n, $t^{n+1/2}$ and t^{n+1}, the source term integration needs the reconstruction of free-surface point-value derivatives $\hat{\eta}'_j$, starting from free-surface point-values $\hat{\eta}_j$. To assure a global fifth-order spatial accuracy,

such a reconstruction must be at least fourth-order accurate. A WENO reconstruction similar to the one described in Section 2.2.2, in which the function $\eta(x)$ is substituted to $K_j(x,u(x,t))$, is used to perform this task.

Finally, the evaluation of the point-values of ξ at each time level is straightforward:

$$\hat{\xi}_j = (gz\,\mathrm{d}\eta/\mathrm{d}x)_j = gz_j\hat{\eta}'_j. \tag{27}$$

2.3.2. Reconstruction of source term integrals

The computation of the integral appearing in Eq. (26) is based on a CWENO reconstruction of the function $\xi(x)$, which is fully consistent with the other reconstructions. This approach is new for several aspects, so it is described in detail in this section.

Introducing $M_{j+1/2}(x)$, suitable polynomials of degree 2, the $\xi(x)$ reconstruction on the staggered grid $I_{j+1/2}$ can be written as:

$$L(x) = \sum_j M_{j+1/2}(x)\chi_{j+1/2}. \tag{28}$$

The cell-averaged values, $\bar{\xi}_{j+1/2}$, on the staggered grid $I_{j+1/2}$ are expressed by:

$$\bar{\xi}_{j+1/2} = \frac{1}{\Delta x}\int_{x_j}^{x_{j+1}} L(x)\,\mathrm{d}x = \frac{1}{\Delta x}\int_{x_j}^{x_{j+1}} M_{j+1/2}(x)\,\mathrm{d}x. \tag{29}$$

In this reconstruction, Eq. (29) plays the same role of Eq. (10) in the staggered cell-averaged variable reconstruction. Notwithstanding this, their structures are quite different. In the case of Eq. (29) the staggered cell-average (related to cell $I_{j+1/2}$) involves only one polynomial cell-reconstruction (related to cell $I_{j+1/2}$), whilst in the case of Eq. (10) the staggered cell-average involves two polynomial cell-reconstructions (related to cells I_j and I_{j+1}).

The reconstruction $L(x)$ is carried out in order to achieve the established order of accuracy and to satisfy the non-oscillation requirement described in Section 2.2.1. Fifth-order spatial accuracy of the source term integrals is obtained imposing the fourth-order accuracy on the cell-averaged value of ξ, i.e.,

$$\frac{1}{\Delta x}\int_{x_j}^{x_{j+1}} L(x)\,\mathrm{d}x = \frac{1}{\Delta x}\int_{x_j}^{x_{j+1}} \xi(x)\,\mathrm{d}x + \mathrm{O}(\Delta x^4). \tag{30}$$

Numerical reconstruction $L(x)$, satisfying (30), is obtained adopting this procedure:

(1) On each cell of the staggered grid $I_{j+1/2}$, two stencils of three adjacent cell-centers of the non-staggered grid x_j, are selected, $\mathscr{N}_{j+m}$, with $m = 0, 1$. Such stencils are centered with respect to the cell boundaries of the cell $I_{j+1/2}$: $\mathscr{N}_{j+m} = \cup_{l=-1}^{l=+1} x_{j+m+l}$.

(2) Two polynomials of degree 2, $N_{j+m}(x)$, with $m = 0, 1$, associated to the stencils $\mathscr{N}_{j+m}$, are defined:

$$N_{j+m}(x) = \tilde{\xi}_{j+m} + \tilde{\xi}'_{j+m}(x - x_{j+m}) + \frac{1}{2}\tilde{\xi}''_{j+m}(x - x_{j+m})^2. \tag{31}$$

Considering the cell-center point-values $\hat{\xi}_{j+m+l}$ with $l = -1, 0, 1$, related to the stencils $\mathscr{N}_{j+m}$, the coefficients of $N_{j+m}(x)$ are determined solving the system:

$$\begin{cases} N_{j+m}(x_{j+m-1}) = \hat{\xi}_{j+m-1}, \\ N_{j+m}(x_{j+m}) = \hat{\xi}_{j+m}, \\ N_{j+m}(x_{j+m+1}) = \hat{\xi}_{j+m+1}, \end{cases} \qquad m = 0, 1. \tag{32}$$

The following coefficients are derived:

$$\begin{aligned} &\tilde{\xi}_{j+m} = \hat{\xi}_{j+m}, \\ &\tilde{\xi}'_{j+m} = \tfrac{1}{2\Delta x}(\hat{\xi}_{j+m+1} - \hat{\xi}_{j+m-1}), \\ &\tilde{\xi}''_{j+m} = \tfrac{1}{2\Delta x^2}(\hat{\xi}_{j+m+1} - 2\hat{\xi}_{j+m} + \hat{\xi}_{j+m-1}), \end{aligned} \qquad m = 0, 1. \tag{33}$$

(3) The third step consists of the reconstruction of a polynomial of degree 3, $Q_{j+1/2}(x)$, defined on the larger stencil of 4 adjacent cell-centers, $\mathcal{Q}_{j+1/2}$, of the non-staggered grid I_j. $\mathcal{Q}_{j+1/2} = \cup_{l=-1}^{l=+2} x_{j+l}$. Such a stencil must include the two previously defined stencils $\mathcal{N}_{j+m}$. Polynomial coefficients evaluation is made following the same procedure explained for the polynomials $N_{j+m}(x)$. Integrating the polynomial $Q_{j+1/2}(x)$ on the cell $I_{j+1/2}$ it is possible to write:

$$\frac{1}{\Delta x}\int_{x_j}^{x_{j+1}} Q_{j+1/2}(x)\,\mathrm{d}x = \frac{1}{\Delta x}\int_{x_j}^{x_{j+1}} \xi(x)\,\mathrm{d}x + \mathrm{O}(\Delta x^4). \tag{34}$$

(4) Considering Eq. (28) and applying WENO method, $L(x)$ reconstruction on the staggered grid $I_{j+1/2}$ is given by a convex combination of the previously defined polynomials $N_{j+m}(x)$:

$$M_{j+1/2}(x) = \sum_{m=0}^{1} w_j^m N_{j+m}(x), \tag{35}$$

where w_j^m, with $m = 0, 1$ are two suitable weights, depending on the smoothness of the solution. The values of the weights, if the solution is regular inside the stencil $\mathcal{Q}_{j+1/2}$, coincide with the values of the linear weights C_m and Eq. (35) becomes:

$$M_{j+1/2}(x) = \sum_{m=0}^{1} C_m N_{j+m}(x). \tag{36}$$

Linear weights are defined in order to satisfy the properties of *convexity* and *symmetry*, described in Section 2.2.1. From these two conditions an univocal set of coefficients is obtained, whose values are reported in Table 1. Linear weights assure the achievement of the prescribed fourth-order of spatial accuracy, too. *Accuracy* condition (30) is verified substituting the set of coefficients C_m in the following relation:

$$\frac{1}{\Delta x}\int_{x_j}^{x_{j+1}} Q_{j+1/2}(x)\,\mathrm{d}x = \sum_{m=0}^{1} C_m \left(\frac{1}{\Delta x}\int_{x_j}^{x_{j+1}} N_{j+m}(x)\,\mathrm{d}x\right) \tag{37}$$

and showing it is an identity. This result proves the effective fourth-order accuracy in space, being:

$$\frac{1}{\Delta x}\int_{x_j}^{x_{j+1}} L(x)\,\mathrm{d}x = \frac{1}{\Delta x}\int_{x_j}^{x_{j+1}} M_{j+1/2}(x)\,\mathrm{d}x = \frac{1}{\Delta x}\int_{x_j}^{x_{j+1}} Q_{j+1/2}(x)\,\mathrm{d}x = \frac{1}{\Delta x}\int_{x_j}^{x_{j+1}} \xi(x)\,\mathrm{d}x + \mathrm{O}(\Delta x^4). \tag{38}$$

(5) To complete the description of this reconstruction, appropriate weights w_j^m must be defined. Referring to (Section 2.2.1), w_j^m depends on solution regularity on $\mathcal{N}_{j+m}$, whose indicator are the indices of smoothness:

$$\mathrm{IS}_j^m = \sum_{l=1}^{2} \int_{I_{j+1/2}} \Delta x^{2l-1} \left(N_{j+m}^{(l)}\right)^2 \mathrm{d}x, \tag{39}$$

whose discretized expressions are:

$$\begin{aligned} \mathrm{IS}_j^0 &= \frac{1}{4}\left(\hat{\xi}_{j+1} - \hat{\xi}_{j-1}\right)^2 + \frac{1}{2}\left[\left(\hat{\xi}_{j+1} - \hat{\xi}_{j-1}\right)\left(\hat{\xi}_{j-1} - 2\hat{\xi}_j + \hat{\xi}_{j+1}\right)\right] + \frac{4}{3}\left(\hat{\xi}_{j-1} - 2\hat{\xi}_j + \hat{\xi}_{j+1}\right)^2, \\ \mathrm{IS}_j^1 &= \frac{1}{4}\left(\hat{\xi}_{j+2} - \hat{\xi}_j\right)^2 - \frac{1}{2}\left[\left(\hat{\xi}_{j+2} - \hat{\xi}_j\right)\left(\hat{\xi}_j - 2\hat{\xi}_{j+1} + \hat{\xi}_{j+2}\right)\right] + \frac{4}{3}\left(\hat{\xi}_j - 2\hat{\xi}_{j+1} + \hat{\xi}_{j+2}\right)^2. \end{aligned} \tag{40}$$

Non-linear weights assume the following expressions:

$$\alpha_j^m = \frac{C_m}{\left(\epsilon + \mathrm{IS}_j^m\right)^p} \quad \text{and} \quad w_j^m = \frac{\alpha_j^m}{\sum_{l=0}^{l=1} \alpha_j^l}. \tag{41}$$

Once $\bar{\xi}_{j+1/2}$ is computed, the cell-averaged source terms can be evaluated using the following equation:

$$\bar{s}_{j+1/2} = \begin{bmatrix} 0 \\ \frac{g}{2\Delta x}\left(z_{j+1}^2 - z_j^2\right) - \frac{g}{\Delta x}\left(\hat{\eta}_{j+1} z_{j+1} - \hat{\eta}_j z_j\right) + \bar{\xi}_{j+1/2} \end{bmatrix}. \tag{42}$$

2.4. C-property verification

In this section the ability of the numerical scheme to satisfies the C-property, i.e., the equality $\bar{u}_j^{n+1} = \bar{u}_j^n$, for $\eta = \eta^* = \text{constant}$ and $vh = 0$, is proved.

2.4.1. The use of SGM

A key element to obtain the balancing is the use of the SGM method [42,33]. As it can be verified through straightforward calculations, such a technique allows, in case of quiescent flow, to obtain that the reconstruction described in Section 2.2.1, starting from $\bar{\eta}_j^n = \eta^* = \text{constant}$ and $\overline{vh}_j^n = 0$, gives $\bar{\eta}_{j+1/2}^n = \hat{\eta}_j^n = \eta^*$ and $\overline{vh}_{j+1/2}^n = \widehat{vh}_j^n = 0$. Similarly, the same reconstruction, starting from $\bar{\eta}_{j+1/2}^{n+1} = \eta^*$ and $\overline{vh}_{j+1/2}^{n+1} = 0$, gives $\bar{\eta}_j^{n+1} = \eta^*$ and $\overline{vh}_j^{n+1} = 0$.

2.4.2. C-property for point-values

The steadiness of the point-value solution (i.e., $\hat{u}^{n+1} = \hat{u}^n$ and $\hat{u}^{n+1/2} = \hat{u}^n$), in case of quiescent flow, must be verified. The time evolution of point-values is described by Eqs. (5) and (7), thus, to achieve this result, it is sufficient to demonstrate that:

$$k_j = 0 \quad \forall j, \tag{43}$$

when $vh = 0$ and $\eta = \text{constant}$.

Due to Eq. (21), in case of quiescent flow, $K_j(x,u)$ is identically zero and so also the point-values $\hat{K}_j(x_{j+k+l}, u_{j+k+l}^{(i)})$, with $k = -1, 0, 1$ and $l = -1, 0, 1$, are zero. Consequently, from Eq. (23), the coefficients of polynomials $P_{j+k}(x)$ are zero and, from Eq. (16), also the coefficients of polynomial $R_j(x)$ are zero. Thus $R_j'(x)$ is a function equal to zero for any x and particularly for x_j. Finally, remembering Eq. (22), the validity of Eq. (43) is proved.

2.4.3. C-property for cell-averages

The steadiness of the cell-averaged solution (i.e., $\bar{u}^{n+1} = \bar{u}^n$), in case of quiescent flow, is verified. To achieve this result, it is sufficient to show that the term in the square brackets of Eq. (3), given Eqs. (42) and (29), is zero at time t^n, $t^{n+1/2}$ and t^{n+1}, for water at rest. Remembering Eqs. (42) and (29) and assuming $\hat{\eta}_j = \hat{\eta}_{j+1} = \eta^* = \text{constant}$ and $vh = 0$, the term in square brackets in (3), for a generic time t, may be written as:

$$\begin{aligned} &\left[f(\hat{u}(x_{j+1},t)) - f(\hat{u}(x_j,t)) - \Delta x \bar{s}_{j+1/2}\right] \\ &= \begin{bmatrix} 0 \\ 1/2g\left(\eta^* - z_{j+1}\right)^2 \end{bmatrix} - \begin{bmatrix} 0 \\ 1/2g\left(\eta^* - z_j\right)^2 \end{bmatrix} - \begin{bmatrix} 0 \\ 1/2g\left(z_{j+1}^2 - z_j^2\right) - g\left(\eta^* z_{j+1} - \eta^* z_j\right) + \Delta x \bar{\xi}_{j+1/2} \end{bmatrix} \\ &= \begin{bmatrix} 0 \\ \Delta x \bar{\xi}_{j+1/2} \end{bmatrix}. \end{aligned} \tag{44}$$

If $\bar{\xi}_{j+1/2}$ are zero then the terms in square brackets are zero. To prove that $\bar{\xi}_{j+1/2}$ are zero in the case of quiescent flow let us consider the following steps. First, if $\hat{\eta}_j$ are constants, then the free-surface derivatives $\hat{\eta}_j'$ (reconstruction in Section 2.3.1) are zero. As a consequence, also the point-values of $\hat{\xi}_j$ are zero. Finally, it is easy to check that if $\hat{\xi}_j$ are zero also the averaged-values $\bar{\xi}_{j+1/2}$, computed using the procedure described in Section 2.3.2, are zero.

3. Applications

In this section numerical results, obtained with the described SWE-CWENO scheme, are reported. The selected test cases allow a detailed analysis of several aspects of the method.

3.1. Accuracy test cases

In this section the effective order of accuracy of the scheme is tested. Two test cases are used: a steady flow over a Gaussian bump and an unsteady flow over a smooth bottom. The former test involves only the spatial accuracy while the latter involves both spatial and time accuracy (see [40]).

3.1.1. Steady flow over a Gaussian bump

The fifth-order spatial accuracy of the scheme is verified using this test case consisting in the simulation of the steady subcritical flow over a Gaussian bump. To study the spatial accuracy separately from the time accuracy and, in particular, to avoid the reduction of the overall accuracy of the scheme due to the time integration procedure, which is fourth-order accurate, only for this test case, Δt^n proportional to $\Delta x^{5/4}$ and $C = 0.35\ \mathrm{m}^{-1/4}$ are assumed. See the work of Vuković et al. [39] for the details.

A 30-m long channel is considered. Bed elevation is defined by a Gaussian function $z(x)$, whose expression is:

$$z(x) = \frac{c_0}{\sigma\sqrt{2\pi}} \mathrm{e}^{-\frac{1}{2}\left(\frac{x-x_m}{\sigma}\right)^2} \tag{45}$$

with $c_0 = 1\ \mathrm{m}^2$, $\sigma = 2$ m and $x_m = 15$ m. A 2-m constant water level and a 0 discharge are the initial conditions. $q = 4.42\ \mathrm{m}^2/\mathrm{s}$ and $h = 2$ m are the upstream and the downstream boundary conditions, respectively. Both the boundary conditions are constant in time. In this test case, $\epsilon = 10^{-6}$ and $p = 2$ are assumed.

Such a test case, in which no discontinuities affect bed elevation and hydraulic variables, has been created ad hoc to perform the accuracy analysis. This analysis is done according to [20,30,13,9]. Therefore, focusing the attention on the free-surface elevation η, the L^1, L^2 and L^∞ norms of the error are computed:

$$\begin{aligned} L^1 &= \sum_{j=1}^{N} \left|\eta(x_j, t^n) - \hat{\eta}_j^n\right| \Delta x, \\ L^2 &= \sqrt{\sum_{j=1}^{N} \left(\eta(x_j, t^n) - \hat{\eta}_j^n\right)^2 \Delta x}, \\ L^\infty &= \max \left|\eta\left(x_j, t^n\right) - \hat{\eta}_j^n\right|, \quad 1 \leqslant j \leqslant N, \end{aligned} \tag{46}$$

where $\eta(x_j,t^n)$ and $\hat{\eta}_j^n$ are the analytical and the numerical point-values of the free-surface elevation, respectively.

In Table 2 the accuracy analysis results, obtained considering four different spatial steps $\Delta x = [0.06, 0.12, 0.24, 0.5]$ m (corresponding to grids of $[500, 250, 125, 60]$ elements), are reported. The fifth-order accuracy is achieved with each norm, confirming that the real spatial accuracy of the scheme coincides with the expected one. Similar results, not reported here, are obtained focusing the attention on the specific discharge.

3.1.2. Unsteady flow over a sinusoidal bump

The fourth-order space and time accuracy of the scheme, achieved in smooth regions of the solution, is verified using the test case proposed by Xing and Shu [40]. Bottom profile is defined by:

$$z(x) = \sin^2(\pi x), \tag{47}$$

Table 2
Gaussian bump test case – accuracy analysis – free-surface elevation

Cells	L^1	Order	L^2	Order	L^∞	Order
60	1.7792E − 03		6.6299E − 04		4.6876E − 04	
125	6.8922E − 05	4.4293	2.8952E − 05	4.2660	2.2966E − 05	4.1093
250	2.6520E − 06	4.6998	1.1336E − 06	4.6747	9.0131E − 07	4.6713
500	8.0789E − 08	5.0368	3.4852E − 08	5.0235	2.7424E − 08	5.0385

while initial conditions are represented by the following expressions:

$$h(x,0) = h_0 + e^{\cos(2\pi x)}; \quad vh(x,0) = \sin(\cos(2\pi x)) \tag{48}$$

with $h_0 = 5$ m and $x \in [0,1]$ m. Periodic boundary conditions are assumed.

This problem cannot be solved analytically and therefore a numerical solution, computed on a very fine mesh of 19,683 cells, is adopted as the reference solution. In this test case, $\epsilon = 10^{-6}$ and $p = 2$ are assumed, as before.

Fig. 1 shows the free surface and the specific discharge after 0.1 s from the start of the simulation. It is clear the good agreement between the reference solution and the numerical solution obtained using the coarser grid.

In Table 3 the accuracy analysis results, computed considering 81, 243, 729, 2187 and 6561 cells are reported. The selected number of cells assures the spatial correspondence of the point-values of the computed solutions with the point-values of the reference solution, simplifying the computation of the norms (46). For any norm, the fourth-order accuracy is achieved, confirming that the accuracy of the scheme agrees with the expected one. Similar results are obtained on the specific discharge.

3.2. C-property test cases

The purpose of this test cases, proposed by Xing and Shu [40], is to verify the achievement of the C-property over non-flat bottom. Two different bottom profiles are chosen:

$$z(x) = 5e^{-\frac{2}{5}(x-5)^2} \text{ m}, \tag{49}$$

which is smooth, and:

$$z(x) = \begin{cases} 4 \text{ m} & \text{if } 4 \leqslant x \leqslant 8 \text{ m}, \\ 0 & \text{otherwise}, \end{cases} \tag{50}$$

which is discontinuous. $0 \leqslant x \leqslant 10$ m for both cases. A constant free-surface elevation, $\eta = 10$ m, and a zero discharge are the initial conditions. This initial quiescent flow must be preserved. To test the ability of the scheme to maintain this state, a simulation is carried out until $t = 0.5$ s, using a mesh of 200 cells, L^1, L^2 and L^∞ norms of the errors of water depth and specific discharge are computed using (46). The results, obtained using the double precision floating-point arithmetics in numerical computation, are summarized in Table 4. The differences of the numerical solution from the reference solution, in terms of water depth and of specific discharge, are due to round-off errors (see [40]). These results prove the satisfaction of the exact C-property.

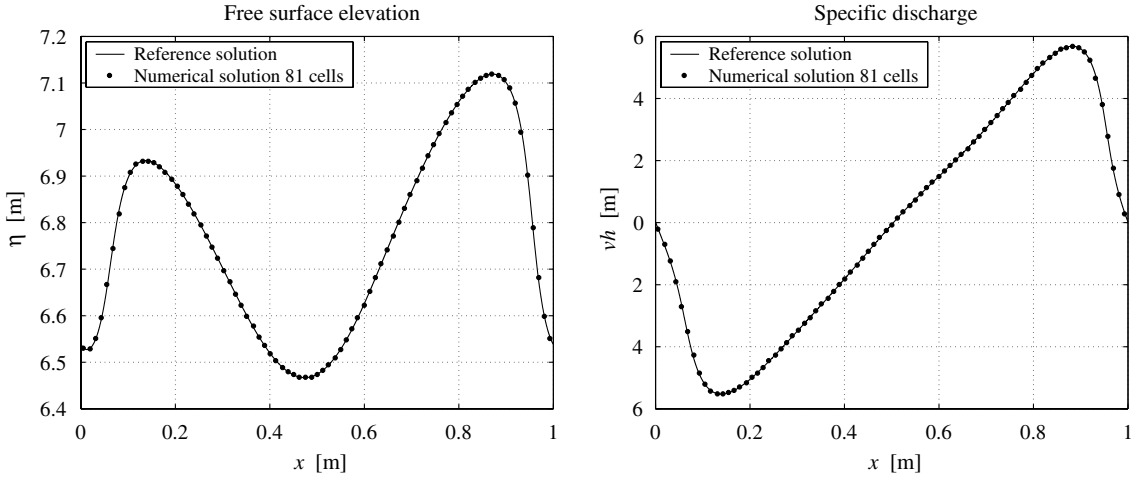

Fig. 1. Unsteady flow over a sinusoidal bump: solution at $t = 0.1$ [s].

Table 3
Unsteady flow over a sinusoidal bump – accuracy analysis – free-surface elevation

Cells	L^1	Order	L^2	Order	L^∞	Order
81	7.2854E − 04		1.9615E − 03		9.7843E − 03	
243	1.3648E − 05	3.6205	5.0621E − 05	3.3288	4.0506E − 04	2.8987
729	1.1443E − 07	4.3522	4.3949E − 07	4.3205	4.2323E − 06	4.1519
2187	1.2328E − 09	4.1240	4.5753E − 09	4.1552	4.3143E − 08	4.1743
6561	1.7159E − 11	3.8908	5.4170E − 11	4.0381	5.0519E − 10	4.0481

3.3. Steady discontinuous flow over a parabolic bump

The purpose of this test case is the validation of the source term treatment for the simulation of steady discontinuous flows over a bump [36,5]. This is a classical test problem for transcritical flows. The spatial domain is a 25 m long channel, discretized with 250 cells ($\Delta x = 0.1$ m). The bottom elevation is described by the following function:

$$z(x) = \begin{cases} 0.2 - 0.05(x-10)^2 \text{ m} & \text{if } 8 \leqslant x \leqslant 12 \text{ m}, \\ 0 & \text{otherwise}, \end{cases} \tag{51}$$

characterized by a discontinuous first derivative in $x = 8$ m and $x = 12$ m. ϵ and p are set equal to 10^{-6} and 2, respectively. The flow is transcritical and a steady shock is located over the bump. The upstream specific discharge is 0.18 m^2/s and the downstream water-surface elevation is set to 0.33 m. The initial free-surface elevation is 0.33 m and the initial discharge is everywhere zero.

Fig. 2 shows the good agreement between the numerical and the analytical solution. The test gives satisfying results in terms of shock resolution and of upstream and downstream water levels reconstruction. The shock position is accurately captured. Only few numerical point-values of flow discharge do not agree well with the analytical solution, but these points are located at the shock position. The comparison with similar numerical results available in the literature [36,5] on the same case test is also satisfactory. The results obtained in this severe test case, in which numerical difficulties due to discontinuous bottom slope and to the discontinuous nature of the solution coexist, support the reliability of the novel source term technique proposed herein.

3.4. Pulse over a bump

This quasi-stationary test case, due to LeVeque [19], is selected in order to test the capability of the scheme in computing an unsteady flow over a smooth bottom profile. It consists of the simulation of the convection of a pulse, initially 0.1 m long and 10^{-3} m height. The pulse moves in a 1 m long domain initially interested by a quiescent flow characterized by a depth of 1 m. The duration of the simulation is 0.7 s. The bottom profile is described by the following equation:

$$z(x) = \begin{cases} 0.25[\cos(10\pi(x-1/2)) + 1] \text{ m} & \text{if } |x - 1/2| < 0.1 \text{ m}, \\ 0 & \text{otherwise}. \end{cases} \tag{52}$$

In this case numerical diffusion is minimized using $\epsilon = 10^{-12}$ and $p = 2$ (see [40]).

The initial disturbance is split in two waves. The left-going wave leaves the domain undisturbed. The right-going wave interacts with the bump. The solutions obtained using 100 and 250 cells are compared with the

Table 4
C-property analysis – water depth and specific discharge norms

Test case	h			vh		
	L^1	L^2	L^∞	L^1	L^2	L^∞
Smooth	3.50E − 15	1.45E − 15	8.88E − 16	3.48E − 13	1.35E − 13	1.05E − 13
Non-smooth	6.66E − 16	5.55E − 16	1.11E − 16	1.08E − 15	2.83E − 15	1.16E − 14

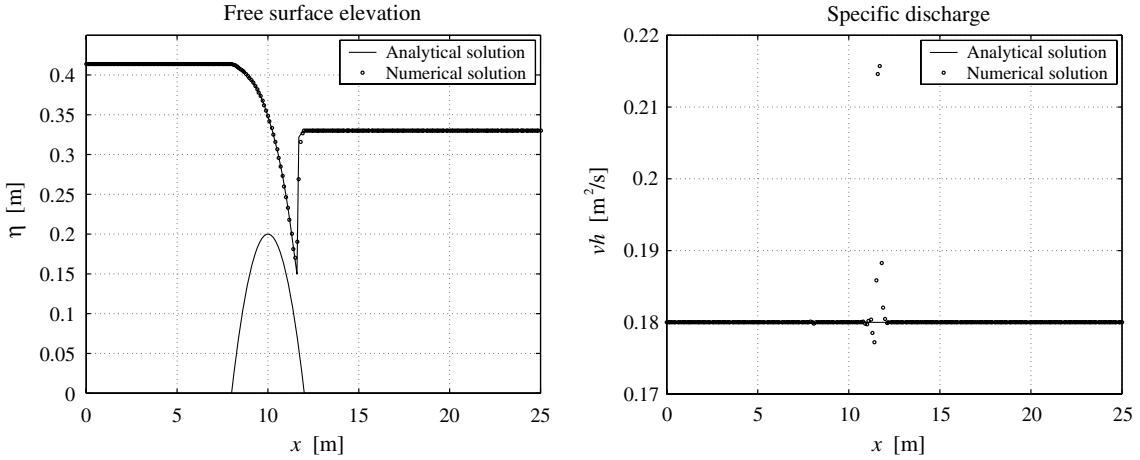

Fig. 2. Parabolic bump-transcritical flow test case.

reference solution obtained using 4000 cells. Moreover, the gravity is set to 1 m/s^2 in order to allow a direct comparison with the results obtained by LeVeque [19]. An overall good behavior of the scheme is shown. In particular, it may be noted the absence of perturbations where the bottom elevation is non-zero and this proves the good balancing between source term and flux gradient in unsteady problems (see Fig. 3).

3.5. Dam-break flow over a rectangular bump

This test case, proposed in [38], is performed to check the ability of the model to simulate rapidly varying flow over discontinuous bottom profiles. Bed elevation is described by the following equation:

$$z(x) = \begin{cases} 8\ \text{m} & \text{if } |x - 750| \leqslant 1500/8\ \text{m}, \\ 0 & \text{otherwise}, \end{cases} \tag{53}$$

defined for $0 \leqslant x \leqslant 1500$ m. The initial conditions are:

$$vh(x,0) = 0 \quad \text{and} \quad \eta(x) = \begin{cases} 20\ \text{m} & \text{if } x \leqslant 750\ \text{m}, \\ 15\ \text{m} & \text{otherwise}. \end{cases} \tag{54}$$

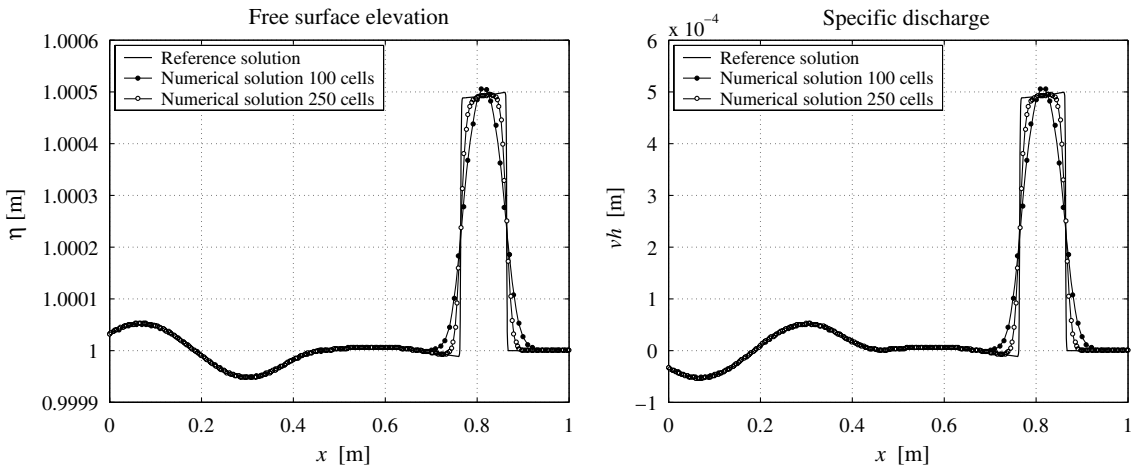

Fig. 3. Pulse over a bump.

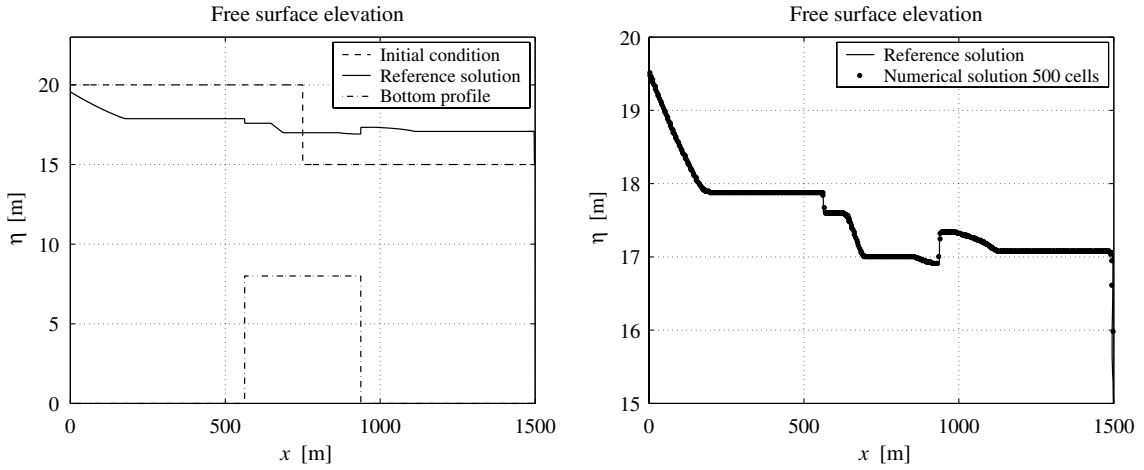

Fig. 4. Dam-break over a rectangular bump.

The duration of the simulation is 60 s. The numerical solution is computed using 500 cells and it is compared, in Fig. 4, with a reference solution computed using 5000 cells. Both the simulations are performed assuming $\epsilon = 10^{-6}$ and $p = 2$. The scheme works well on this test case. The resolution of the solution discontinuities, located on the wave front and on the bottom steps, are very good. The solution is non-oscillatory and it agrees well with the reference one.

4. Conclusions

The class of central WENO schemes represents a versatile, efficient and robust tool for the integration of hyperbolic systems of balance laws. For these characteristics central WENO schemes are particularly interesting from the engineering point of view.

In this work a new well-balanced scheme, belonging to the family of central WENO methods, fourth-order accurate in space and time, suitable for the integration of shallow water equation with bottom slope source term, is presented. The attention is focused on a new approach for the geometrical source term treatment, which allows to satisfy the exact C-property for the quiescent flows over non-flat bottom profiles, preserving the fourth-order time and space accuracy of the original homogeneous CWENO methods. To achieve this aim two original well-balanced WENO reconstructions are introduced: one for the point-value flux derivative and one for the source term spatial integration.

Several test problems are used to check the space and time accuracy, the exact C-property, the non-oscillatory property and the resolution of the shocks.

Acknowledgment

We are grateful to Professor Lorenzo Pareschi of the Department of Mathematics, University of Ferrara, for the useful suggestions and discussions.

References

[1] F. Alcrudo, P. Garcia-Navarro, A high-resolution Godunov-type scheme in finite volumes for the 2D shallow-water equations, International Journal of Numerical Methods in Fluids 16 (1993) 489–505.
[2] P. Arminjon, A. St-Cyr, Nessyahu Tadmor-type central finite volume methods without predictor for 3D cartesian and unstructured tetrahedral grids, Applied Numerical Mathematics 46 (2003) 135–155.
[3] A. Bermudez, M.E. Vázquez-Cendón, Upwind methods for hyperbolic conservation laws with source terms, Computers and Fluids 23 (8) (1994) 1049–1071.
[4] S. Bryson, D. Levy, Balanced central schemes for shallow water equations on unstructured grids, SIAM Journal of Scientific Computation 27 (2) (2005) 532–552.

[5] V. Caleffi, A. Valiani, A. Zanni, Finite volume method for simulating extreme flood events in natural channels, IAHR Journal of Hydraulic Research 41 (2) (2003) 167–177.
[6] L. Fraccarollo, H. Capart, Riemann wave description of erosional dam-break flows, Journal of Fluid Mechanics 461 (2002) 183–228.
[7] P. Garcia-Navarro, M.E. Vázquez-Cendón, On numerical treatment of the source terms in shallow water equations, Computers and Fluids 29 (2000) 951–979.
[8] S.K. Godunov, A difference scheme for numerical computation of discontinuous solution of hydrodynamic equations, Mathematics of the USSR-Sbornik 43 (1959) 271–306.
[9] A. Harten, B. Engquist, S. Osher, S.R. Chakravarthy, Uniformly high-order accurate essentially non-oscillatory schemes, III, Journal of Computational Physics 71 (2) (1987) 231–475.
[10] M.E. Hubbard, P. Garcia-Navarro, Flux difference splitting and the balancing of source terms and flux gradients, Journal of Computational Physics 165 (1) (2000) 89–125.
[11] P.P. Jansen, L. Van Bendegom, J. Van den Berg, M. De Vries, A. Zanen, Principles of River Engineering, the Non-Tidal Alluvial River, Pitman Publishing Ltd., London, 1979.
[12] G.S. Jiang, D. Levy, C.T. Lin, S. Osher, E. Tadmor, High-resolution nonoscillatory central schemes with nonstaggered grids for hyperbolic conservation laws, SIAM Journal on Numerical Analysis 35 (6) (1998) 2147–2168.
[13] G.S. Jiang, C.W. Shu, Efficient implementation of weighted ENO schemes, Journal of Computational Physics 126 (1) (1996) 202–228.
[14] G.S. Jiang, E. Tadmor, Non-oscillatory central schemes for multidimensional hyperbolic conservation laws, SIAM Journal on Scientific Computing 19 (6) (1998) 1892–1917.
[15] H. Kikkawa, S. Ikeda, A. Kitagawa, Flow and bed topography in curved open channels, ASCE Journal of Hydraulics Division 102 (9) (1976) 1327–1342.
[16] A. Kurganov, S. Noelle, G. Petrova, Semi-discrete central-upwind scheme for hyperbolic conservation laws and Hamilton–Jacobi equations, SIAM Journal of Scientific Computation 23 (2001) 707–740.
[17] A. Kurganov, G. Petrova, Central-upwind schemes on triangular grids for hyperbolic systems of conservation laws, Numerical Methods for Partial Differential Equations 21 (3) (2005) 536–552.
[18] P.D. Lax, Weak solutions of nonlinear hyperbolic equations and their numerical computations, Communications of Pure and Applied Mathematics 44 (1954) 21–41.
[19] R.J. LeVeque, Balancing source terms and flux gradients in high-resolution Godunov methods: the quasi-steady wave-propagation algorithm, Journal of Computational Physics 146 (1) (1998) 346–365.
[20] D. Levy, G. Puppo, G. Russo, Central WENO schemes for hyperbolic systems of conservation laws, Mathematical Modelling and Numerical Analysis 33 (3) (1999) 547–571.
[21] D. Levy, G. Puppo, G. Russo, A fourth-order central WENO scheme for multidimensional hyperbolic systems of conservation laws, SIAM Journal on Scientific Computing 24 (2) (2002) 480–506.
[22] J.A. Liggett, Fluid Mechanics, McGraw-Hill, New York, 1994.
[23] X.D. Liu, S. Osher, T. Chan, Weighted essentially non-oscillatory schemes, Journal of Computational Physics 115 (1) (1994) 200–212.
[24] C.G. Mingham, D.M. Causon, High-resolution finite-volume method for shallow water flows, ASCE Journal of Hydraulic Engineering 124 (6) (1998) 605–614.
[25] H. Nessyahu, E. Tadmor, Non-oscillatory central differencing for hyperbolic conservation laws, Journal of Computational Physics 87 (2) (1990) 408–463.
[26] S. Noelle, W. Rosenbaum, M. Rumpf, 3D adaptive central schemes: Part I. Algorithms for assembling the dual mesh, Applied Numerical Mathematics (accepted for publication).
[27] L. Pareschi, G. Puppo, G. Russo, Central Runge–Kutta schemes for conservation laws, SIAM Journal on Scientific Computing 26 (3) (2005) 979–999.
[28] J. Qiu, C.W. Shu, On the construction, comparison, and local characteristic decomposition for high-order central WENO schemes, Journal of Computational Physics 183 (1) (2002) 187–209.
[29] I.L. Rozovskii, Flow of water in bends of open channels. Technical Report, Academy of Sciences of the Ukrainian S.S.R., Institute of Hydrology and Hydraulic Engineering, Kiev, 1957.
[30] C.W. Shu, Essentially non-oscillatory and weighted essentially non-oscillatory schemes for hyperbolic conservation laws, ICASE Technical Report 97-65, NASA, Langley Research Center, Hampton, VA, USA, 1997.
[31] J.V. Soulis, Computation of two-dimensional dambreak flood flows, International Journal of Numerical Methods in Fluids 14 (1992) 631–664.
[32] E. Toro, Riemann problems and the WAF method for solving the two-dimensional shallow water equations, Philosophical Transactions of the Royal Society A338 (1992) 43–68.
[33] N. Črnjarić-Žic, S. Vuković, L. Sopta, Balanced finite volume WENO and central WENO schemes for the shallow water and the open-channel flow equations, Journal of Computational Physics 200 (2) (2004) 512–548.
[34] A. Valiani, L. Begnudelli, Divergence form for bed slope source term (DFB) in shallow water equations, ASCE Journal of Hydraulic Engineering (2006) (to appear).
[35] A. Valiani, V. Caleffi, A. Bernini, Central WENO schemes for shallow water movable bed equations, in: 12th International Conference on Transport and Sedimentation of Solid Particles, vol. 2, Prague, Czech Republic, September 2004, Institute of Hydrodynamics, Academy of Sciences of the Czech Republic, pp. 651–658.
[36] A. Valiani, V. Caleffi, A. Zanni, Case study: Malpasset dambreak simulation using a 2D finite volume method, ASCE Journal of Hydraulic Engineering 128 (5) (2002) 460–472.

[37] M.E. Vázquez-Cendón, Improved treatment of source terms in upwind schemes for the shallow water equations in channels with irregular geometry, Journal of Computational Physics 148 (2) (1999) 497–526.
[38] S. Vuković, L. Sopta, ENO and WENO schemes with the exact conservation property for one-dimensional shallow water equations, Journal of Computational Physics 179 (2) (2002) 593–621.
[39] S. Vuković, N. Ćrnjarić-Žic, L. Sopta, WENO schemes for balance laws with spatially varying flux, Journal of Computational Physics 199 (1) (2004) 87–109.
[40] Y. Xing, C.W. Shu, High order finite difference WENO schemes with the exact conservation property for the shallow water equations, Journal of Computational Physics 208 (1) (2005) 206–227.
[41] M. Zennaro, Natural continuous extension of Runge–Kutta methods, Mathematics of Computation 46 (1986) 119–133.
[42] J.G. Zhou, D.M. Causon, D.M. Ingram, C.G. Mingham, The surface gradient method for the treatment of source terms in the shallow-water equations, Journal of Computational Physics 168 (1) (2001) 1–25.
[43] J.G. Zhou, D.M. Causon, D.M. Ingram, C.G. Mingham, Numerical solutions of the shallow water equations with discontinuous bed topography, International Journal for Numerical Methods in Fluids 38 (8) (2002) 769–788.